LETTER TO THE EDITOR

An extended *Herschel* drop-out source in the center of AS1063: a normal dusty galaxy at *z* = 6.1 or SZ substructures?

F. Boone[1,2], B. Clément[3], J. Richard[4], D. Schaerer[5,2], D. Lutz[6], A. Weiß[7], M. Zemcov[8], E. Egami[3], T. D. Rawle[9], G. L. Walth[3], J.-P. Kneib[10,11], F. Combes[12], I. Smail[13], A. M. Swinbank[13], B. Altieri[9], A. W. Blain[14], S. Chapman[15], M. Dessauges-Zavadsky[5], R. J. Ivison[16], K. K. Knudsen[17], A. Omont[18], R. Pelló[1,2], P. G. Pérez-González[19], I. Valtchanov[9], P. van der Werf[20], and M. Zamojski[5]

[1] Université de Toulouse, UPS-OMP, IRAP, 31028 Toulouse, France
e-mail: frederic.boone@irap.omp.eu
[2] CNRS, IRAP, 9 Av. colonel Roche, BP 44346, 31028 Toulouse Cedex 4, France
[3] Steward Observatory, University of Arizona, 933 North Cherry Avenue, Tucson, AZ 85721, USA
[4] Centre de Recherche Astrophysique de Lyon, Université Lyon 1, 9 avenue Charles André, 69561 Saint-Genis-Laval, France
[5] Geneva Observatory, Université de Genève, 51 chemin des Maillettes, 1290 Versoix, Switzerland
[6] Max-Planck-Institut für extraterrestrische Physik, Postfach 1312, 85741 Garching, Germany
[7] Max-Planck-Institut für Radioastronomie, Auf dem Hügel 69, 53121 Bonn, Germany
[8] Department of Physics, Mathematics, and Astronomy, California Institute of Technology, Pasadena, CA 91125, USA
[9] European Space Astronomy Centre (ESAC)/ESA, Villanueva de la Cañada, 28691 Madrid, Spain
[10] Laboratoire d'astrophysique, École Polytechnique Fédérale de Lausanne, Observatoire de Sauverny, 1290 Versoix, Switzerland
[11] Aix-Marseille Université, CNRS, LAM, UMR 7326, 13388 Marseille, France
[12] LERMA, Observatoire de Paris, 61 avenue de l'Observatoire, 75014 Paris, France
[13] Institute for Computational Cosmology, Department of Physics, Durham University, Durham DH1 3LE, UK
[14] Physics & Astronomy, University of Leicester, Leicester, LE1 7RH, UK
[15] Department of Physics and Atmospheric Science, Dalhousie University Halifax, NS, B3H 3J5, Canada
[16] Institute for Astronomy, University of Edinburgh, Royal Observatory, Blackford Hill, Edinburgh EH9 3HJ, UK
[17] Department of Earth and Space Science, Chalmers University of Technology, Onsala Space Observatory, 43992 Onsala, Sweden
[18] UPMC Univ Paris 6, UMR 7095, Institut d'Astrophysique de Paris, 75014 Paris, France
[19] Departamento de Astrofísica, Facultad de CC. Físicas, Universidad Complutense de Madrid, 28040 Madrid, Spain
[20] Leiden Observatory, Leiden University, PO box 9513, 2300 RA Leiden, The Netherlands

ABSTRACT

In the course of our 870 μm APEX/LABOCA follow-up of the *Herschel* Lensing Survey we have detected a source in AS1063 (RXC J2248.7-4431) that has no counterparts in any of the *Herschel* PACS/SPIRE bands, it is a *Herschel* "drop-out" with $S_{870}/S_{500} \geq 0.5$. The 870 μm emission is extended and centered on the brightest cluster galaxy, suggesting either a multiply imaged background source or substructure in the Sunyaev-Zel'dovich increment due to inhomogeneities in the hot cluster gas of this merging cluster. We discuss both interpretations with emphasis on the putative lensed source. Based on the observed properties and on our lens model we find that this source may be the first submillimeter galaxy (SMG) with a moderate far-infrared (FIR) luminosity ($L_{FIR} < 10^{12} L_\odot$) detected so far at $z > 4$. In deep HST observations we identified a multiply imaged $z \sim 6$ source and measured its spectroscopic redshift to be $z = 6.107$ with VLT/FORS. This source may be associated with the putative SMG, but it is most likely offset spatially by $10-30$ kpc and they may be interacting galaxies. With a FIR luminosity in the range $[5-15] \times 10^{11} L_\odot$ corresponding to a star formation rate in the range $[80-260] M_\odot$ yr^{-1}, this SMG would be more representative of the $z > 4$ dusty galaxies than the extreme starbursts detected so far. With a total magnification of ~25 it would open a unique window to the normal dusty galaxies at the end of the epoch of reionization.

Key words. galaxies: high-redshift – galaxies: star formation – galaxies: evolution – submillimeter: galaxies

1. Introduction

Estimating the contribution of dust-obscured star formation in the early Universe is essential to constrain the models of galaxy evolution and has been a growing field of research since the late 1990s (e.g., Blain et al. 2002). Owing to the negative *K*-correction, distant dusty galaxies (also known as submillimeter galaxies, SMGs) were efficiently detected in submillimeter (submm) surveys and their redshift distribution was found to peak at $z \sim 2-3$ (Chapman et al. 2005).

With the advent of the new generation of submm instruments the hunt for the highest-redshift SMGs progressed at a rapid pace in recent years. The first SMG beyond $z = 5$ was discovered by Capak et al. (2011) with JCMT/AzTEC. Based on a *Herschel* detection and a 30 m/EMIR follow-up, Combes et al. (2012) discovered an interacting system of bright SMGs at $z = 5.243$. At the same time, Walter et al. (2012) used IRAM instruments and found that an SMG known for years in the Hubble deep field is actually a system of galaxies lying at $z = 5.2$. Following-up on SPT bolometer observations, Vieira et al. (2013), and Weiß et al. (2013) measured the spectroscopic redshifts of 23 new SMGs

Table 1. Photometry of the 870 μm northern peak with the wavelengths (λ) given in μm and the flux densities (S_ν) in mJy.

λ	24	70	100	160	250	350	500	870
S_ν	<0.06	<0.75	<1.2	<3.8	<7.2	<9.9	<12.3	7.6 ± 1.1

Notes. The upper limts are at 3σ.

with ALMA. Of these, two are at $z > 5$. In parallel, Riechers et al. (2013) observed red SMGs based on *Herschel* colors with CARMA and discovered the highest-redshift SMG at $z = 6.34$.

In terms of luminosity, however, all SMGs detected so far beyond $z > 4$ are ultraluminous infrared galaxies[1] (ULIRGs) with $L_{FIR} > 10^{12} L_\odot$ or even hyperluminous infrared galaxies (HyLIRGs) with $L_{FIR} > 10^{13} L_\odot$, implying star formation rates $SFRs \gtrsim 10^3 M_\odot \, yr^{-1}$. As confirmed by recent ALMA number counts (Karim et al. 2013; Hatsukade et al. 2013), these extreme starbursts are not representative of the average population of dusty star-forming galaxies at $z > 4$, and the luminous infrared galaxies (LIRGs) with $L_{FIR} \sim 10^{11} L_\odot$ that should represent the majority are yet to be discovered. The lensing power provided by massive galaxy clusters is widely used to detect distant galaxies (e.g., Smail et al. 1997). However, the recent discovery of substructures in the Sunyaev-Zel'dovich (SZ) increment of interacting clusters (Korngut et al. 2011; Mroczkowski et al. 2012) may complicate the interpretation of submm observations. We report here the discovery of a good candidate for a normal star forming-galaxy at $z = 6.1$ lensed by the cluster AS1063 (RXCJ2248.7-4431) and discuss the possibility that this source may instead correspond to substructures in the SZ effect. We adopt the ΛCDM concordance cosmology: $H_0 = 71 \, km \, s^{-1} \, Mpc^{-1}$, $\Omega_M = 0.27$ and $\Omega_\Lambda = 0.73$.

2. Observations and data reduction

Herschel observations of AS1063 at 70, 100, 160, 250, 350, and 500 μm were obtained as part of the *Herschel* Lensing Survey (program IDs: KPOT_eegami_1, OT2_trawle_3) as described by Egami et al. (2010) and Rawle et al. (2010). The full widths at half maximum (FWHM) of the beams are 5.2″, 7.7″, 11.3″,18.1″, 24.9, and 36.6″, respectively.

Observations of AS1063 at 870 μm with the Large APEX Bolometer Camera (LABOCA, Siringo et al. 2009) were obtained in the frame of the LABOCA Lensing Survey, a large program coordinated by ESO and the MPI (E187A0437A, M-087.F-0005-2011). The observations were carried out in April and May 2012 in excellent weather conditions with an average precipitable water vapor (PWV) of 0.5 mm. The spiral mapping pattern was chosen to cover a circular area of ~8′ in diameter centered on the clusters. Absolute flux calibration was achieved through observations of Mars, Uranus, and Neptune as well as secondary calibrators and was found to be accurate to within ~10% (rms). The atmospheric attenuation was determined via skydips about every 2 h and also from independent data from the APEX radiometer which measures the line-of-sight water vapor column every minute (see Siringo et al. 2009, for a more detailed description). Pointing was checked on the nearby quasars and was found to be stable within 3″ (rms). The data were reduced using the bolometer array data analysis software (BoA Schuller 2012). The effective resolution of the maps is 24.3″. The pixel noise rms at the center of the map is 1.1 mJy beam^{-1}.

[1] The lowest-luminosity SMG detected so far at $z > 4$ has $L_{FIR} = 1.3 \times 10^{12} L_\odot$ and is located at $z = 4.04$ (Knudsen et al. 2010).

3. Results

The LABOCA map shows a source at the center of cluster AS1063 (Fig. 1) that is extended at the resolution of LABOCA (beam *FWHM* = 24.3″) and centered on the brightest cluster galaxy (BCG). Its northeastern part has no counterparts in any of the *Herschel* bands or in the 24 μm MIPS band; it is a very red *Herschel* drop-out. It peaks at 7.6 ± 1.1 mJy and its 3-σ upper limit at 500 μm is 13 mJy, implying a flux ratio $S_{870}/S_{500} \geq 0.5$.

Although the BCG is not detected with *Herschel* (Rawle et al. 2012), the southwestern part of the 870 μm source is partly blended with the emission from two lower-redshift sources with spectroscopic redshifts $z = 0.6$ and 0.3 (Walth et al., in prep.). To extract the source properties in this crowded field we applied a multiwavelength simultaneous fit of the maps assuming a modified black-body spectral energy distribution (SED) shape (following Blain et al. 2003, with $\alpha = 2.9$ and $\beta = 1.5$) for all the sources. There are two free parameters per source, corresponding to the FIR luminosity and the wavelength of the SED peak (determined by the dust temperature, T_d and the redshift z). In a first iteration we ran the procedure with the two low-z sources only. The residuals are shown with green contours in Fig. 2; they represent the 870 μm foreground-deblended emission. The morphology and the distribution of this emission with respect to the critical lines, with two peaks on each side of the BCG – one to the northeast at 7.6 mJy and the other to the southwest at 5.3 mJy – suggest either a multiply imaged background source or substructures in the SZ increment. We discuss the two interpretations in turn in the following section.

4. Discussion

4.1. Photometry of a putative lensed source

In a second iteration we ran the photometry procedure again to simultaneously fit two sources at the positions of the 870 μm peaks in addition to the two low-z sources. We assumed that the two 870 μm sources are the images of a single lensed source, which implies a unique peak wavelength (same redshift and dust temperature) and a total of seven free parameters. The χ^2 value gives us an indication of the quality of the fit, it is plotted against the redshift and the dust temperature of the lensed source in Fig. 3 with contours indicating the confidence levels. At a given dust temperature, the 870 μm flux and the *Herschel* upper limits impose a lower limit to the redshift. Thus, if we assume $T_d > 20 \, K$, as observed in most SMGs including those with the lowest luminosities (see, e.g. Symeonidis et al. 2013; Magnelli et al. 2012; or Swinbank et al. 2010) the source must be at $z \gtrsim 2$. If $T_d = 30 \, K$ (mean value for $L_{FIR} \sim 10^{11.5} L_\odot$ according to the same references), the redshift must be ≥ 4. In addition, if we assumed $z < 7$, the observed (i.e., uncorrected for lensing) FIR luminosities of the two peaks must be $<10^{13} L_\odot$ (Fig. 3).

4.2. Lens and source models

Based on the identification of 13 multiple-image systems, five of which have a spectroscopic redshift and the others have a reliable photometric redshift, we built a lens model of the cluster (Richard et al., in prep.). The critical lines computed with this model for $z = 6$ are shown in Fig. 2 as red lines.

As shown in the left panel of Fig. 2, we can reproduce the two 870 μm peaks by assuming a single source modeled by a circular Gaussian of *FWHM* = 2 kpc at $z = 6$. Four images of the source, labeled L1, L2, L3, and L4, are actually formed in a classical quad configuration; their magnifications are 10.8, 3.7, 7.1, and 3.1, respectively, for a total magnification $\mu = 24.7$.
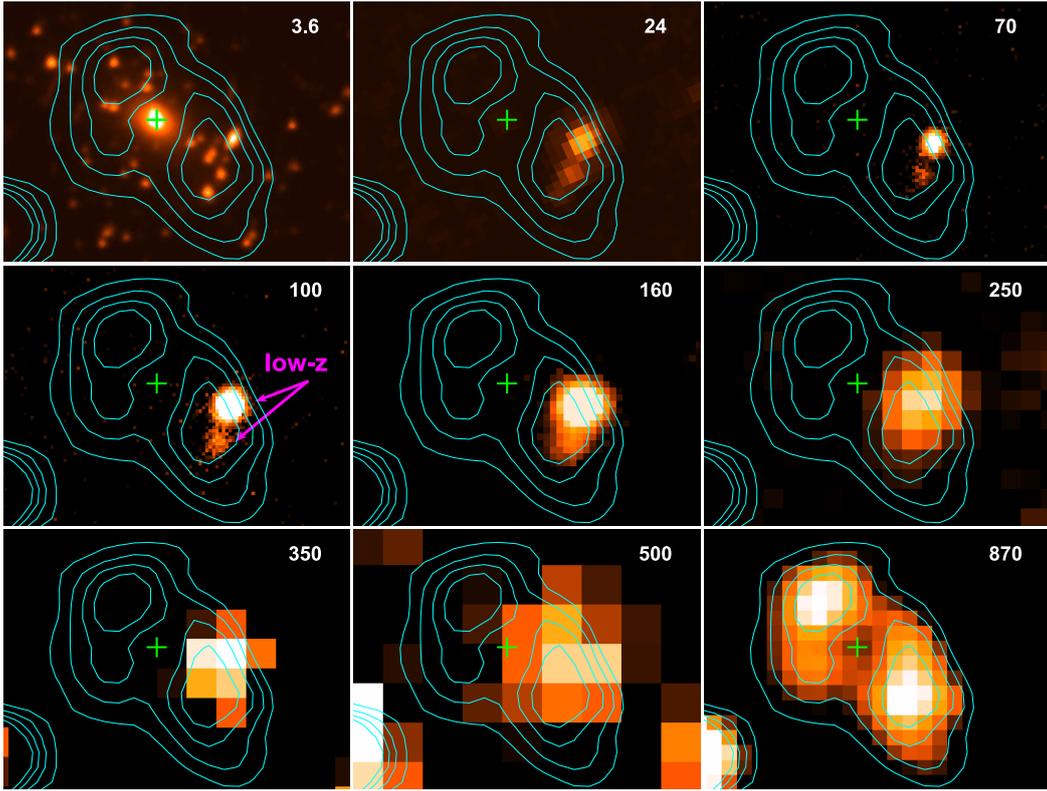
Fig. 1. $105'' \times 78''$ thumbnails showing the central region of the cluster AS1063 at 3.6, 24, 70, 100, 160, 250, 350, 500, and 870 μm (*from left to right* and *from top to bottom*). The contours correspond to the 870 μm emission detected with LABOCA at 3, 4, 5 and 6-σ (σ = 1.1 mJy). The *Herschel* drop-out source can be seen around the BCG (marked by the green cross) at the center of the 870 μm map. The arrows in the 100 μm map point at two low-z sources (z = 0.3 and 0.6), whose 870 μm emission is blended with the southwestern part of the high-z source.
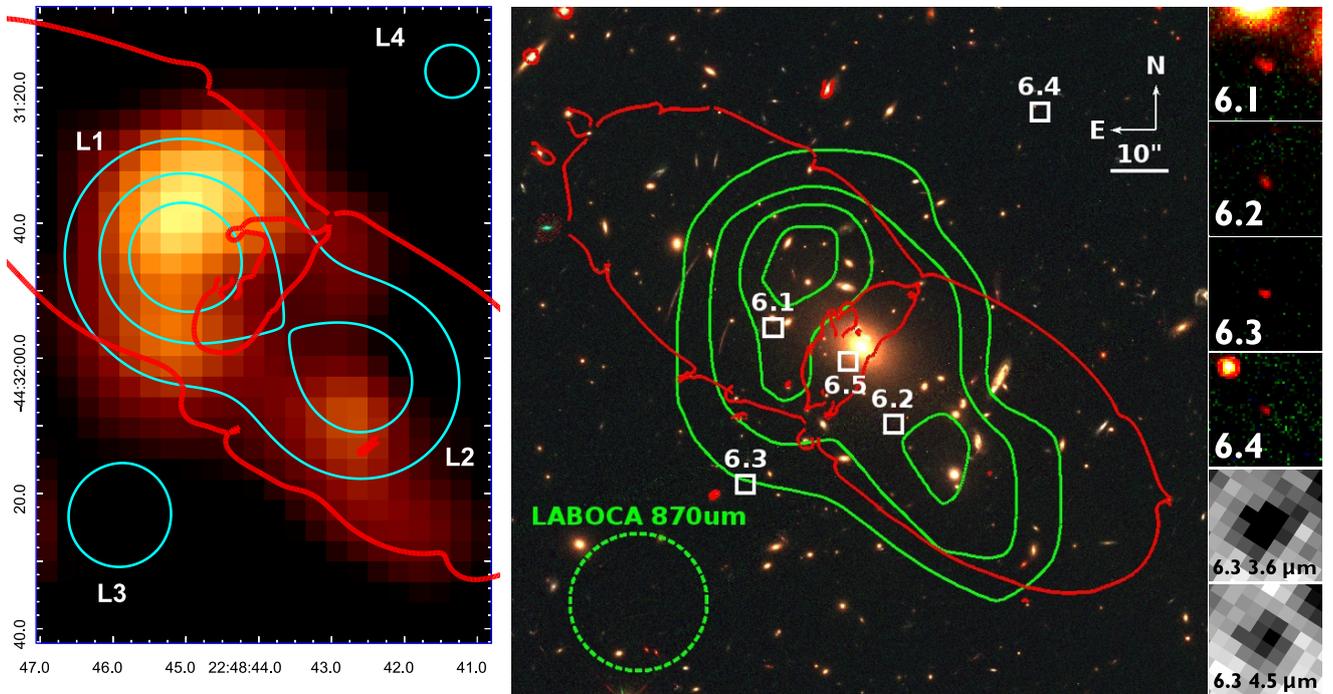
Fig. 2. *Left*: residuals of the 870 μm emission after subtracting the two low-z sources. The cyan contours represent the $z = 6$ source model lensed by the cluster and observed at the resolution of LABOCA. The four images formed are labeled L1, L2, L3, and L4. The contour levels are at 0.25, 0.5 and 0.75 $\times S_{L1}$, where S_{L1} is the peak flux of the L1 image. The critical lines for $z = 6$ are overlaid in red. *Right*: HST color image of the cluster center of AS1063 assembled from images in the filters F606W (blue), F775W (green) and F125W (red). The white squares show the positions of the 4 images of a $z = 6.1$ background source. The thumbnails at the right are $3'' \times 3''$ zooms into these 4 images. The green contours show the 870 μm emission at 2.6, 3.9, 5.2, and 6.5 mJy (RMS = 1.1 mJy). The dotted green circle represents the LABOCA beam (*FWHM* = 24.3$''$).
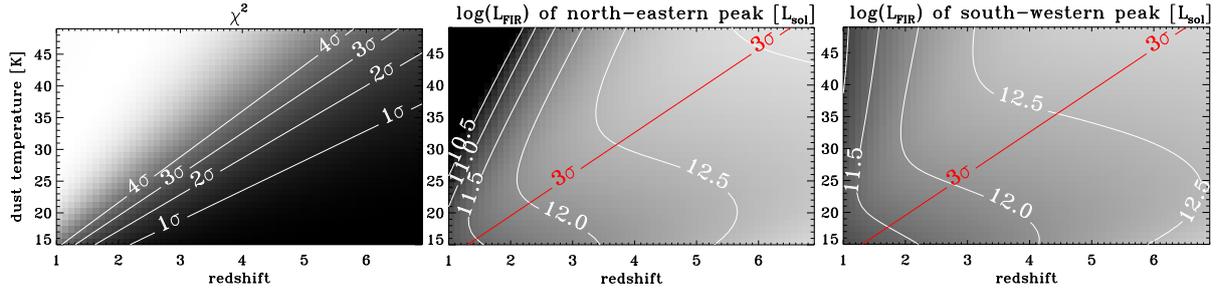
Fig. 3. *Left panel*: χ^2 map in the z-T_d plane, where z and T_d are the redshift and the dust temperature assumed for the 870 μm source detected with LABOCA. The two 870 μm peaks shown in Fig. 2 and the two low-z sources (at $z = 0.6$ and 0.3) shown in Fig. 1 are fitted simultaneously at all wavelengths from 100 to 870 μm assuming a modified black-body SED for each source (7 free parameters). The white contours show the 1σ, 2σ, 3σ, and 4σ confidence levels. *Middle and right panels*: best-fit FIR luminosity in log without any lensing correction in the z-T_d plane for the two 870 μm peaks. The white contours are spaced by 0.5 dex. The χ^2 3σ confidence level is overplotted in red.
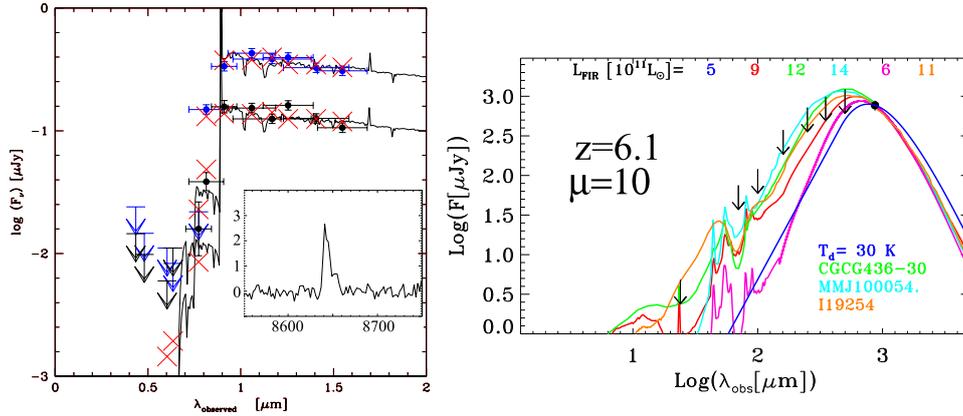

Fig. 4. *Left*: SED fits to the HST/ACS-WFC3 photometry of the images B and D (A is contaminated by a nearby source, C is in a noisy strip of the detector). The best fits give $z = 6.3 \pm 0.3$. The inset shows the VLT/FORS spectrum of the B image with the Ly-α line clearly detected at $z = 6.107$ (Richard et al., in prep.). The x-axis of the inset corresponds to the observed wavelength in Å. *Right*: SED fits to the 870 μm northern peak taking into account the upper limits listed in the Table 1 and assuming $z = 6.1$ and $\mu = 10$ (all the fluxes are corrected for magnification). The modified black-body SED with $T_d = 30$ K is shown in blue, it gives a FIR luminosity $L_{\rm FIR} = 5 \times 10^{11} L_\odot$. The other templates come from the the Chary & Elbaz (2001) library (red), the Vega et al. (2008) library (green), the Michałowski et al. (2010a,b) library (cyan), and the Polletta et al. (2007) library (orange). The template in magenta corresponds to the SMM J2135-0102 model (Swinbank et al. 2010; Ivison et al. 2010).

The images L3 and L4 are $\sim 3\times$ fainter than L1 and are therefore at $\sim 2\sigma$, which is consistent with no detection. To obtain an L1-image brighter than the others it needs to be aligned with a galaxy of the cluster such that it undergoes an additional magnification. In this model the L1-image is formed close to two galaxies of the cluster. The differences between the model and the data are $\leq 3\sigma$. Because the angular distance between the two peaks (L1 and L2) decreases with decreasing redshift, our lens model puts a strong constraint on the redshift, which must be ≥ 4 if we assume a single source. We note that it is possible that the southern source arises from lensing of a second background galaxy, but this would imply multiple sources with similar very red SEDs.

Hence, according to our lens+source model and to the photometry, the luminosity of the putative lensed source corrected for lensing is most likely $< 10^{12} L_\odot$, which is an order of magnitude lower than that of SMGs detected at $z > 4$ so far. For example, if we assume $T_d = 30$ K and $z = 6$, the observed luminosity of the northern peak is $L_{\rm FIR} \sim 5 \times 10^{12} L_\odot$ (middle panel of Fig. 3), with $\mu_{\rm L1} = 10$ this implies an intrinsic luminosity $L_{\rm FIR} \sim 5 \times 10^{11} L_\odot$.

4.3. A plausible HST counterpart at z = 6.107

In the HST images and catalogs provided by the CLASH project we identified four objects (named 6.1, 6.2, 6.3 and 6.4, in Fig. 2

as in Richard et al., in prep.), which might be the four images of a high-z source. Indeed, fitting various SED templates to the HST photometry, we derived a redshift $z = 6.3 \pm 0.3$ (Fig. 4) and the image positions were accurately reproduced by our lens model for a source at $z \sim 6$. To confirm the redshift we recently obtained VLT/FORS spectroscopy of the 6.2, 6.3, and 6.4 images. The Ly-α line is clearly detected at $z = 6.107$ (Fig. 4)[2]. The magnifications are $\mu_{6.1} = 17.1$, $\mu_{6.2} = 6.7$, $\mu_{6.3} = 5.9$, and $\mu_{6.4} = 2.5$.

The image 6.1 of this HST source benefits from a boost by the same two galaxies of the cluster as in the model discussed above for the 870 μm emission. However, if they are both at the same redshift the LABOCA source needs to be offset from the HST source to reproduce the southern peak (L2); it is at ~ 30 kpc in the above model. The distance between the two sources is mainly constrained by the flux ratio of the two 870 μm peaks, it may be in the range 10–30 kpc, suggesting interacting galaxies.

The SFR of the HST source estimated from the UV continuum and from the Ly-α line and corrected for lensing are

---

[2]   Recently Bradley et al. (2013) mentioned a quintuple system in this cluster, but they listed only three of our identified images (6.1, 6.3, and 6.4). After the submission of our letter two other articles appeared online (Monna et al. 2013; Balestra et al. 2013) that describe this system in more detail and provide a similar spectroscopic redshift. We confirm the fifth image identified by these authors and show it in Fig. 2 as 6.5.
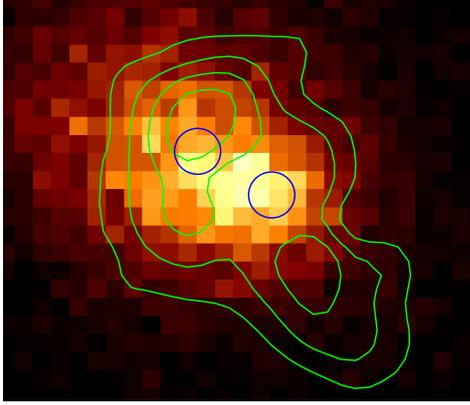
Fig. 5. *Chandra* X-ray map of AS1063 overlaid with the LABOCA residuals in green contours starting at 2σ and spaced by 1σ. The blue circles mark the positions of the two components of the β-model fitted by Gómez et al. (2012) to the *Chandra* data.

$SFR_{UV} \sim 5\,M_\odot\,\mathrm{yr}^{-1}$ and $SFR_{Ly\alpha} \sim 15\,M_\odot\,\mathrm{yr}^{-1}$. The *Spitzer* detection of 6.3 at 3.6 μm implies (H-3.6) $\approx$ 2, redder than for typical $z \sim 6-8$ LBGs (McLure et al. 2011). SED fits with young populations predict up to $A_v \sim 1.5$, implying a reprocessed IR luminosity of $\sim 4 \times 10^{11} L_\odot$, that is an $SFR_{IR} \sim 70\,M_\odot\,\mathrm{yr}^{-1}$.

At $z = 6.1$ the upper limit on the FIR luminosity of the 870 μm source depends on the SED template assumed, as illustrated in the right panel of Fig. 4. The intrinsic luminosities obtained are in the range $[5-15] \times 10^{11} L_\odot$, which corresponds to an SFR in the range $[80-260]\,M_\odot\,\mathrm{yr}^{-1}$. The star-forming properties of the HST and the LABOCA sources may therefore be similar.

4.4. SZ substructure in the merging cluster?

AS1063 is known to produce a strong SZ effect (Plagge et al. 2010), which was detected at $S/N \sim 17$ with *Planck* (Planck Collaboration 2013b). Furthermore, Gómez et al. (2012) showed that this cluster is undergoing a major merging event close to the plane of the sky, and there has been growing evidence in recent years, both from observations and simulations, that such a merging configuration can produce small-scale substructures in the SZ (Korngut et al. 2011; Mroczkowski et al. 2012; Ruan et al. 2013). These substructures may be caused by shocks and inhomogeneities in the hot gas and their increment could peak at $300-400$ GHz (i.e., $750-1000\,\mu$m, Ruan et al. 2013). The SED of these SZ substructures may therefore be consistent with the *Herschel* and LABOCA photometry. We also note that the northern LABOCA peak is close to the secondary mass component identified by Gómez et al. (2012) (Fig. 5), and its elongated morphology would be consistent with shocked gas. The large-scale SZ would be filtered out by the LABOCA observations and the data reduction, and we would be seeing the substructures related to the merging event. More quantitatively, the measurement from the *Planck* nominal survey (Planck Collaboration 2013a) at 353 GHz is 0.12 MJy/sr. It can be used to scale the SZ profile modeled by Plagge et al. (2010) for this cluster and thus estimate the peak flux expected at the center of the LABOCA map, ignoring spatial filtering. We obtain ~ 7 mJy/beam. The fraction of this flux filtered by the observations is difficult to estimate from the data because it depends on the morphology of the SZ increment. This will be studied in a forthcoming paper by Zemcov et al. (in prep.).

5. Conclusion

With APEX/LABOCA we have detected an extended 870 μm source aligned with the center of the cluster AS1063. The source is not detected at shorter FIR/submm wavelengths. We found two possible interpretations of this peculiar source: it may be the dusty component of an HST-detected strongly lensed galaxy at $z = 6.1$ or substructures in the SZ effect. The current observations do not allow us to conclude in favor of one of the two interpretations.

There are two routes to decide between the different origins of the features we discovered: submm observations with ALMA are expected to allow us to resolve the four images of the high-z source, while lower-frequency observations (150 GHz) are required to measure the decrement of the SZ substructures.

References

Balestra, I., Vanzella, E., Rosati, P., et al. 2013, A&A, accepted [arXiv:1309.1593]
Blain, A. W., Smail, I., Ivison, R. J., Kneib, J.-P., & Frayer, D. T. 2002, Phys. Rep., 369, 111
Blain, A. W., Barnard, V. E., & Chapman, S. C. 2003, MNRAS, 338, 733
Bradley, L. D., Zitrin, A., Coe, D., et al. 2013, ApJ, submitted [arXiv:1308.1692]
Capak, P. L., Riechers, D., Scoville, N. Z., et al. 2011, Nature, 470, 233
Chapman, S. C., Blain, A. W., Smail, I., & Ivison, R. J. 2005, ApJ, 622, 772
Chary, R., & Elbaz, D. 2001, ApJ, 556, 562
Combes, F., Rex, M., Rawle, T. D., et al. 2012, A&A, 538, L4
Egami, E., Rex, M., Rawle, T. D., et al. 2010, A&A, 518, L12
Gómez, P. L., Valkonen, L. E., Romer, A. K., et al. 2012, AJ, 144, 79
Hatsukade, B., Ohta, K., Seko, A., Yabe, K., & Akiyama, M. 2013, ApJ, 769, L27
Ivison, R. J., Swinbank, A. M., Swinyard, B., et al. 2010, A&A, 518, L35
Karim, A., Swinbank, A. M., Hodge, J. A., et al. 2013, MNRAS, 432, 2
Knudsen, K. K., Kneib, J.-P., Richard, J., Petitpas, G., & Egami, E. 2010, ApJ, 709, 210
Korngut, P. M., Dicker, S. R., Reese, E. D., et al. 2011, ApJ, 734, 10
Magnelli, B., Lutz, D., Santini, P., et al. 2012, A&A, 539, A155
McLure, R. J., Dunlop, J. S., de Ravel, L., et al. 2011, MNRAS, 418, 2074
Michałowski, M., Hjorth, J., & Watson, D. 2010a, A&A, 514, A67
Michałowski, M. J., Watson, D., & Hjorth, J. 2010b, ApJ, 712, 942
Monna, A., Seitz, S., Greisel, N., et al. 2013, MNRAS, submitted [arXiv:1308.6280]
Mroczkowski, T., Dicker, S., Sayers, J., et al. 2012, ApJ, 761, 47
Plagge, T., Benson, B. A., Ade, P. A. R., et al. 2010, ApJ, 716, 1118
Planck Collaboration 2013a, A&A, submitted [arXiv:1303.5062]
Planck Collaboration 2013b, A&A, submitted [arXiv:1303.5089]
Polletta, M., Tajer, M., Maraschi, L., et al. 2007, ApJ, 81
Rawle, T. D., Chung, S. M., Fadda, D., et al. 2010, A&A, 518, L14
Rawle, T. D., Edge, A. C., Egami, E., et al. 2012, ApJ, 747, 29
Riechers, D. A., Bradford, C. M., Clements, D. L., et al. 2013, Nature, 496, 329
Ruan, J. J., Quinn, T. R., & Babul, A. 2013, MNRAS, 432, 3508
Schuller, F. 2012, in SPIE Conf. Ser., 8452
Siringo, G., Kreysa, E., Kovács, A., et al. 2009, A&A, 497, 945
Smail, I., Ivison, R. J., & Blain, A. W. 1997, ApJ, 490, L5
Swinbank, A. M., Smail, I., Longmore, S., et al. 2010, Nature, 464, 733
Symeonidis, M., Vaccari, M., Berta, S., et al. 2013, MNRAS, 431, 2317
Vega, O., Clemens, M. S., Bressan, A., et al. 2008, A&A, 484, 631
Vieira, J. D., Marrone, D. P., Chapman, S. C., et al. 2013, Nature, 495, 344
Walter, F., Decarli, R., Carilli, C., et al. 2012, Nature, 486, 233
Weiß, A., De Breuck, C., Marrone, D. P., et al. 2013, ApJ, 767, 88